



In-situ resin infiltration of 3D printed porous structures

K. Chen^a, W. Jiang^a, Li^{b,*}, Li H. ^c, C. Wang^d, J. Li^e, F. Li^e, S. Wang^f, K. J. Essler^f, Li L. ^f, J. Gao^f, T. P. Jijun^f

^aGemological Institute, China University of Geosciences, Wuhan 430074, PR China
^bHubei Gem and Jewelry Engineering Technology Research Center, Wuhan 430074, PR China
^cSchool of Materials Science and Engineering, Huazhong University of Science and Technology, Wuhan 430074, PR China
^dMechanical Engineering, University of Birmingham, Birmingham B15 2TT, UK
^eSchool of Electrical and Electronic Engineering, Huazhong University of Science and Technology, Wuhan 430074, PR China
^fWMG, Materials Engineering Centre, University of Warwick, CV4 7AL Coventry, UK

ARTICLE INFO

Keywords:

3D printing
Composite materials
Infiltration
Porous structures
Electromagnetic shielding

ABSTRACT

Currently, three-dimensional (3D) printing is still a relatively slow and expensive process, and the surface quality of the printed parts is poor. However, the development of three-dimensional (3D) printing technology has led to the emergence of in-situ resin infiltration (CVD) technology. In this paper, a 3D printed porous structure is infiltrated with resin using CVD technology. The results show that the resin infiltration rate of 3D printed porous structures is significantly higher than that of traditional porous structures. The resin infiltration rate of 3D printed porous structures is 88% and 27% higher than that of traditional porous structures. The electromagnetic interference (EMI) shielding effectiveness (SE) of the 3D printed porous structures is significantly higher than that of traditional porous structures. The SE of the 3D printed porous structures is 47.8 dB at 2.7 GHz and 32.3 dB at 2–18 GHz. The results show that the 3D printed porous structures have a significant advantage in terms of EMI shielding effectiveness.

1. Introduction

Generally, the resistance of sp^2 carbon materials, such as carbon fibers, carbon nanotubes, and carbon nanofibers, is significantly higher than that of sp^3 carbon materials, such as diamond and silicon carbide [1]. The electrical conductivity of carbon materials is also significantly higher than that of sp^3 carbon materials [2]. However, the strength of carbon materials is significantly lower than that of sp^3 carbon materials [3]. After the development of 3D printing technology, the strength of 3D printed porous structures is significantly higher than that of traditional porous structures [4]. The electrical conductivity of 3D printed porous structures is also significantly higher than that of traditional porous structures [5].

(2DG), the electrical conductivity is significantly higher than that of traditional porous structures [6,7]. The results show that the 3D printed porous structures have a significant advantage in terms of EMI shielding effectiveness [8]. The results show that the 3D printed porous structures have a significant advantage in terms of EMI shielding effectiveness [9]. The results show that the 3D printed porous structures have a significant advantage in terms of EMI shielding effectiveness [10]. The results show that the 3D printed porous structures have a significant advantage in terms of EMI shielding effectiveness [11]. The results show that the 3D printed porous structures have a significant advantage in terms of EMI shielding effectiveness [12]. However, the strength of 3D printed porous structures is still significantly lower than that of traditional porous structures [13]. The results show that the 3D printed porous structures have a significant advantage in terms of EMI shielding effectiveness [14]. The results show that the 3D printed porous structures have a significant advantage in terms of EMI shielding effectiveness [15]. Most of the 3D printed porous structures have a significant advantage in terms of EMI shielding effectiveness [16]. By the way, the 3D printed porous structures have a significant advantage in terms of EMI shielding effectiveness [17].

*Corresponding author. E-mail address: ylj@uig.edu.cn (Y. Li).

t lyst. T i es e i t isti s (i ., e esitie i e-
 st t), t t i i fl e t fi l i est t
 (i ., l y t i ss, f ts) e f t 3DG. B si s, t -
 t 3DG i i t t e e t i s f e t t l t l t
 (i ., e esity, e si s, f lity). H e , est e f t e es
 t l t l t s y e t i e l t e s i ffi lty
 i e sly l t i e esity, f e i st , t e i l Ni f e
 lly st e esity y e l y e t e l l f e i t
 e t t, t s s tly e t i 3DG s e s e e t e l e f e-
 s e i i e s e i f t s f e s i f i f t i e l s i 17,18].
 H e , it is e f ssity t e l e t l t l t s, i
 i s l y i l t f e e t e i e s t s t e i 3DG i t
 t l st t s s t l f e s 19].
 S l t i l s l t i (SLM), s i e t i i t i -
 f t i (AM) t e l e y, i s t i l l y s i f e t f i t i e
 e f s e l s t i t / e i s t - i s i e l (3D) t l t l t s
 i t t t s e f e l i t y i s i , f f i i y i e t i e
 f l i lity e f *in-situ* f t i i lity. T e t , e s
 s s e t SLM e e s s t t s e f T i l l e y s 20],
 s t i l s l l e y s 21], N i l l e y s 22]. C i s t e s t i l y s f e l /
 s s t t f e l - s y t s i i s t t - e f t - t -
 s i s t i l s. C e i t N i e e t s s t t ,
 e i s s e s i l s s t t f e e t
 i CVD t e t l e e s t t i e l l (< 0.001 t.%)
 e t e s s s l f - l i t i e f e , i t t e t i -
 lity s i l l y i t l s 23]. W i l N i s
 i e s e l i lity (> 0.1 t.%) 17], t i f i l s t
 t e f e s e f s s i e i t i e 24]. H e , -
 s i SLM e f e i s s t i l l i t s i f y s e f i s f f i i t
 t i f e e s l t i i f e i t s i t i s i i t l
 e t i lity f l t i lity t e s e e l s l t
 (1000–1100). F i t i e e f i s e s e s f f e l s
 i SLM i s s t i l l f i y l l s 25].
 T e e e l i t i e s, f e t f i s t t i e e s
 f s i l e t t e - e t e e 3DG/ e (3DG/C) s t -
 t s i SLM s i l t e sly i e i t i e i t CVD e t e f
 . A l l - s i y e i - t y e e s e t l t s
 i t i l l y i s t i t i SLM f e i e s t t l e l t i e t e -
 e s e i f e , s i l l y i t s t t e i s e t e y 0 081 i t i

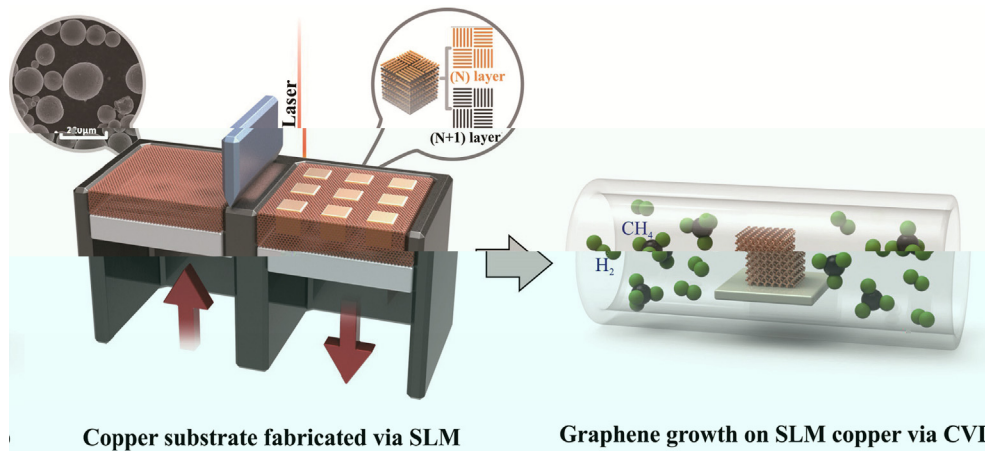


Fig. 1. Illustration of the 3DG/C porous substrate fabrication process followed by *in-situ* graphene growth via CVD. (For interpretation of the references to this figure legend, the reader is referred to the web version of this article.)

ASTM B193-2002 is used to measure the tensile strength of the samples. The tensile strength is measured at a crosshead speed of $(5 \sim 10 \times 10^{-3})$ mm/min according to ASTM E1461-2013 using a universal testing machine (LFA (Laser Flash Analyzer), Netzsch LFA457, Germany). The test specimens (SENTERRA, Böhler, Germany) are tested at a 3DG/C substrate thickness of 514 μm . The test specimens (S11 and S21) are tested at a temperature of 1000 $^{\circ}\text{C}$ using a VNA (Anton Paar PNA-N5244A, USA) with a frequency range of 2–18 GHz. The test specimens are sectioned, and the sectioned specimens are used for SEM and EDS analysis.

3. Results and discussion

3.1. Formation of SLM copper

3.1.1. SLM manufacturing of copper under different line energy densities

The test specimens are fabricated under different line energy densities. Different

types of specimens are used to measure the tensile strength of the samples (Fig. 2). The tensile strength is measured at a crosshead speed of $(5 \sim 10 \times 10^{-3})$ mm/min according to ASTM E1461-2013 using a universal testing machine (LFA (Laser Flash Analyzer), Netzsch LFA457, Germany). The test specimens (SENTERRA, Böhler, Germany) are tested at a 3DG/C substrate thickness of 514 μm . The test specimens (S11 and S21) are tested at a temperature of 1000 $^{\circ}\text{C}$ using a VNA (Anton Paar PNA-N5244A, USA) with a frequency range of 2–18 GHz. The test specimens are sectioned, and the sectioned specimens are used for SEM and EDS analysis.

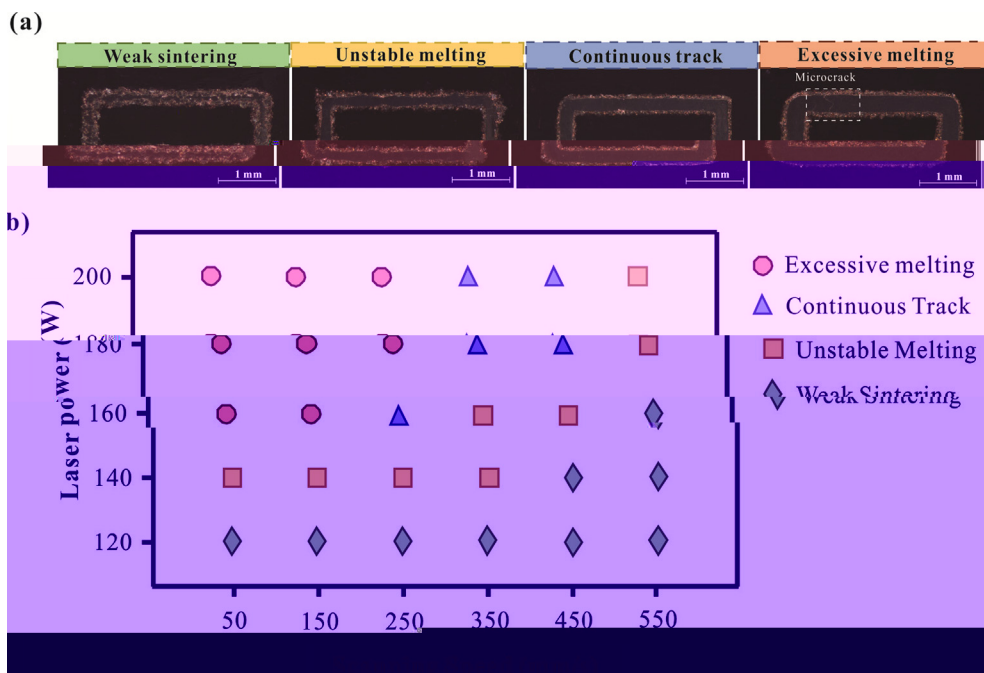


Fig. 2. (a) Typical morphology of the specimens showing different melting states: (a) Weak sintering; (b) Unstable melting; (c) Continuous track; (d) Excessive melting. (For interpretation of the references to this figure legend, the reader is referred to the web version of this article.)

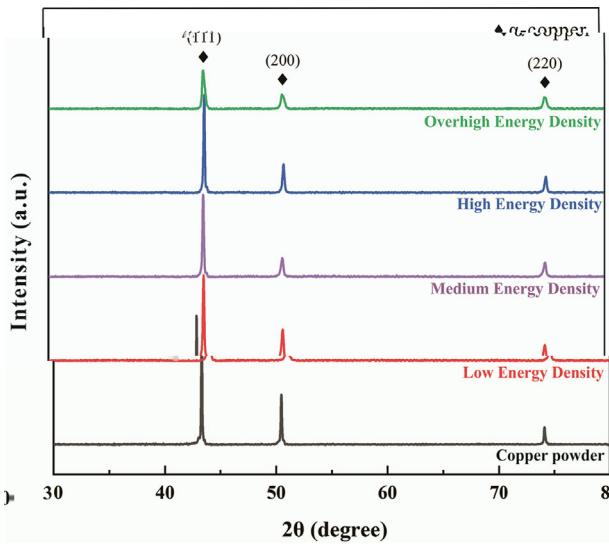


Fig. 3. XRD patterns of copper powder at different energy densities. (For interpretation of the references to colour in this figure legend, the reader is referred to the web version of this article.)

3.1.2. Formation of anisotropic microstructure under different volumetric energy density

The XRD patterns of copper powder at different energy densities are shown in Fig. 3. The (111) and (200) peaks shift to $2\theta = 43.32^\circ$ and $2\theta = 50.45^\circ$, respectively (Fig. 3), and the (111) peak intensity is significantly higher than that of the other two peaks. This indicates that the copper powder has a strong (111) preferred orientation. The intensity of the (111) peak increases with increasing energy density, indicating that the (111) preferred orientation becomes stronger. This is due to the fact that the laser energy density affects the grain growth and orientation of the copper powder during the SLM process. In addition, the intensity of the (200) peak also increases with increasing energy density, indicating that the (200) preferred orientation also becomes stronger. This is due to the fact that the laser energy density affects the grain growth and orientation of the copper powder during the SLM process.

The XRD patterns of copper powder at different energy densities are shown in Fig. 3. The (111) and (200) peaks shift to $2\theta = 43.32^\circ$ and $2\theta = 50.45^\circ$, respectively (Fig. 3), and the (111) peak intensity is significantly higher than that of the other two peaks. This indicates that the copper powder has a strong (111) preferred orientation. The intensity of the (111) peak increases with increasing energy density, indicating that the (111) preferred orientation becomes stronger. This is due to the fact that the laser energy density affects the grain growth and orientation of the copper powder during the SLM process. In addition, the intensity of the (200) peak also increases with increasing energy density, indicating that the (200) preferred orientation also becomes stronger. This is due to the fact that the laser energy density affects the grain growth and orientation of the copper powder during the SLM process.

The XRD patterns of copper powder at different energy densities are shown in Fig. 3. The (111) and (200) peaks shift to $2\theta = 43.32^\circ$ and $2\theta = 50.45^\circ$, respectively (Fig. 3), and the (111) peak intensity is significantly higher than that of the other two peaks. This indicates that the copper powder has a strong (111) preferred orientation. The intensity of the (111) peak increases with increasing energy density, indicating that the (111) preferred orientation becomes stronger. This is due to the fact that the laser energy density affects the grain growth and orientation of the copper powder during the SLM process. In addition, the intensity of the (200) peak also increases with increasing energy density, indicating that the (200) preferred orientation also becomes stronger. This is due to the fact that the laser energy density affects the grain growth and orientation of the copper powder during the SLM process.

The XRD patterns of copper powder at different energy densities are shown in Fig. 3. The (111) and (200) peaks shift to $2\theta = 43.32^\circ$ and $2\theta = 50.45^\circ$, respectively (Fig. 3), and the (111) peak intensity is significantly higher than that of the other two peaks. This indicates that the copper powder has a strong (111) preferred orientation. The intensity of the (111) peak increases with increasing energy density, indicating that the (111) preferred orientation becomes stronger. This is due to the fact that the laser energy density affects the grain growth and orientation of the copper powder during the SLM process. In addition, the intensity of the (200) peak also increases with increasing energy density, indicating that the (200) preferred orientation also becomes stronger. This is due to the fact that the laser energy density affects the grain growth and orientation of the copper powder during the SLM process.

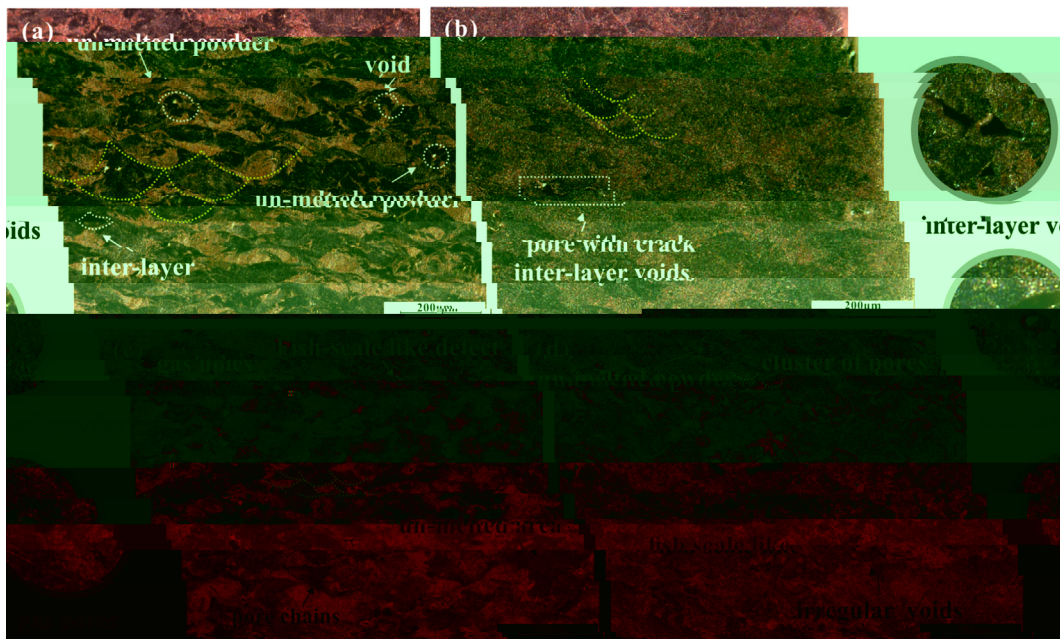


Fig. 4. SEM micrographs of copper powder at different energy densities: (a) (3000 J/cm³), (b) (857 J/cm³), (c) (285 J/cm³), (d) (128 J/cm³), respectively. (For interpretation of the references to colour in this figure legend, the reader is referred to the web version of this article.)

t i t e t e t s e i e i e t.

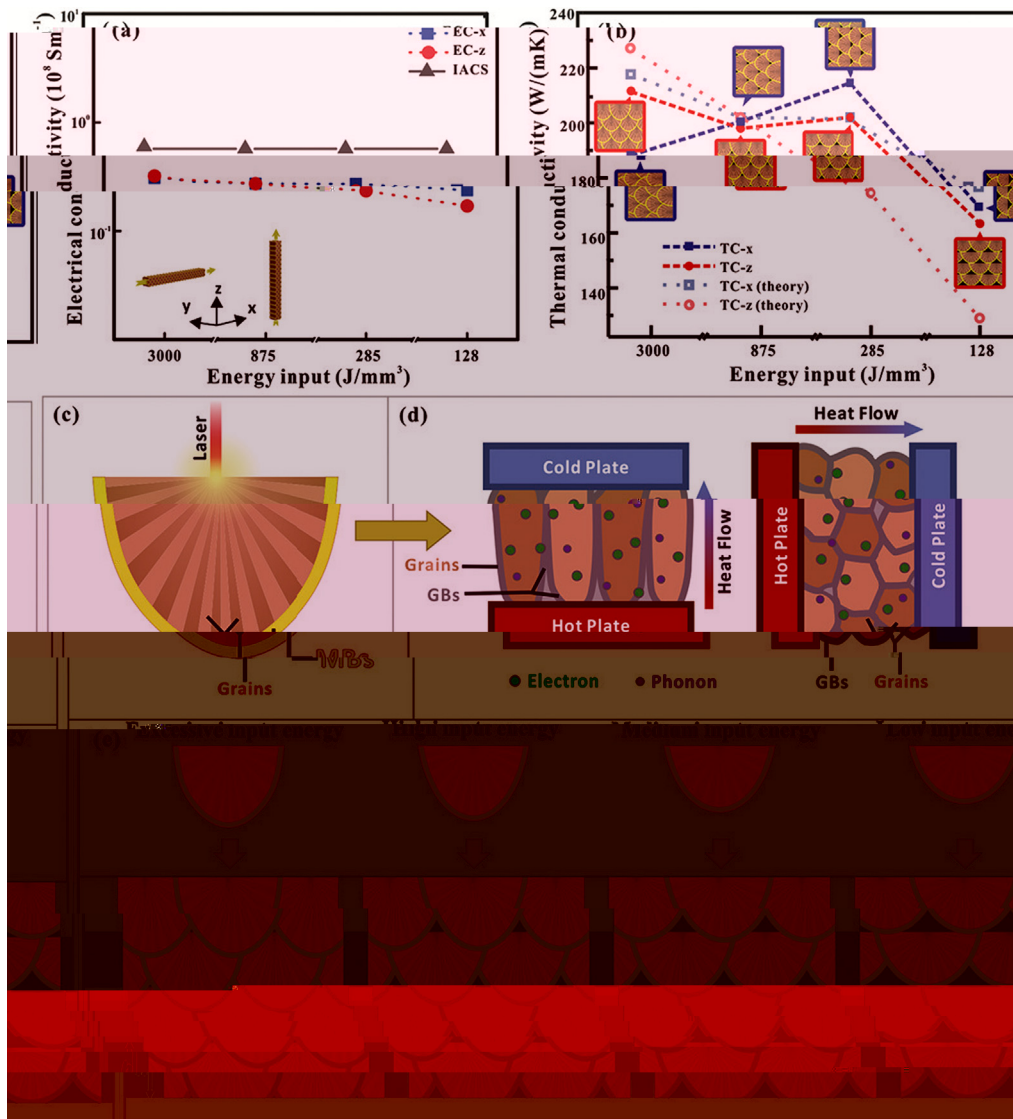


Fig. 7. (a) Electrical conductivity (b) Thermal conductivity (c) Schematic of laser irradiation (d) Schematic of heat flow through the scaffold.

is a key factor for the design of the scaffold.

3.3. Morphology and structure of CVD 3DG/Cu porous scaffolds

The porous scaffolds with different densities were fabricated by the laser-assisted CVD method. As the laser power and the distance between the laser and the scaffold were adjusted, the morphology and structure of the scaffolds were significantly affected [39]. A porous scaffold with a density of 33% was prepared by laser-assisted CVD at 25 V and 25 W [39]. Using the same method, porous scaffolds with different densities (10%, 20%, 30%, 40%, 50%, 60%, 70%, 80%, 90%) were prepared [40]. The porous scaffolds were characterized by SEM, TEM, and EDS. The porous scaffolds were composed of Cu and Ni, Li [40]. The porous scaffolds were composed of Cu and Ni, Li [40]. The porous scaffolds were composed of Cu and Ni, Li [40]. The porous scaffolds were composed of Cu and Ni, Li [40].

At the same time, the porous scaffolds were characterized by SEM, TEM, and EDS. The porous scaffolds were composed of Cu and Ni, Li [40]. The porous scaffolds were composed of Cu and Ni, Li [40]. The porous scaffolds were composed of Cu and Ni, Li [40]. The porous scaffolds were composed of Cu and Ni, Li [40]. The porous scaffolds were composed of Cu and Ni, Li [40]. The porous scaffolds were composed of Cu and Ni, Li [40]. The porous scaffolds were composed of Cu and Ni, Li [40]. The porous scaffolds were composed of Cu and Ni, Li [40]. The porous scaffolds were composed of Cu and Ni, Li [40].

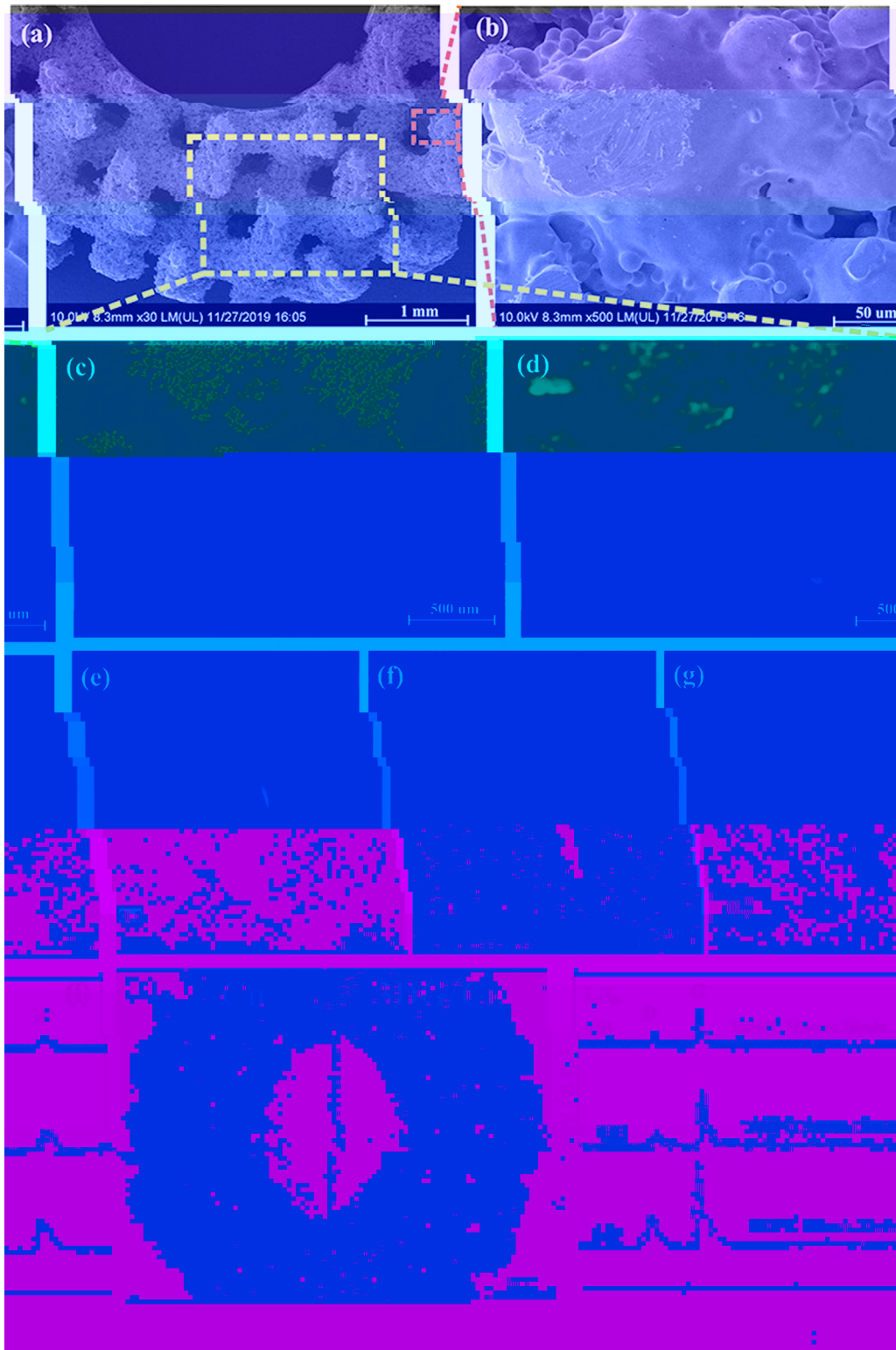


Fig. 8. (a) SEM image of 3DG/C porous scaffold; (b) SEM image of 3DG/C porous scaffold; (c) EDS image of 3DG/C porous scaffold; (d) EDS line scan profile of 3DG/C porous scaffold; (e) EDS spectrum of 3DG/C porous scaffold; (f) EDS spectrum of Cu; (g) EDS spectrum of C.

The density of foams with respect to the theoretical density of foams, I_D/I_G is in the range of 0.71 to 0.93, indicating that the foams are highly porous. The foams were prepared by the foaming process at 1000 °C, for 30 s, in a furnace of 20 MPa.

3.4. Thermal property and EMI shielding effectiveness of 3DG/Cu porous scaffolds

The thermal stability of the 3DG/Cu porous scaffolds was evaluated by TGA. The weight loss of the 3DG/Cu porous scaffolds was 26.8% at 2000 °C, and the weight loss of the 3DG/C porous scaffolds was 14.8% at 2000 °C.

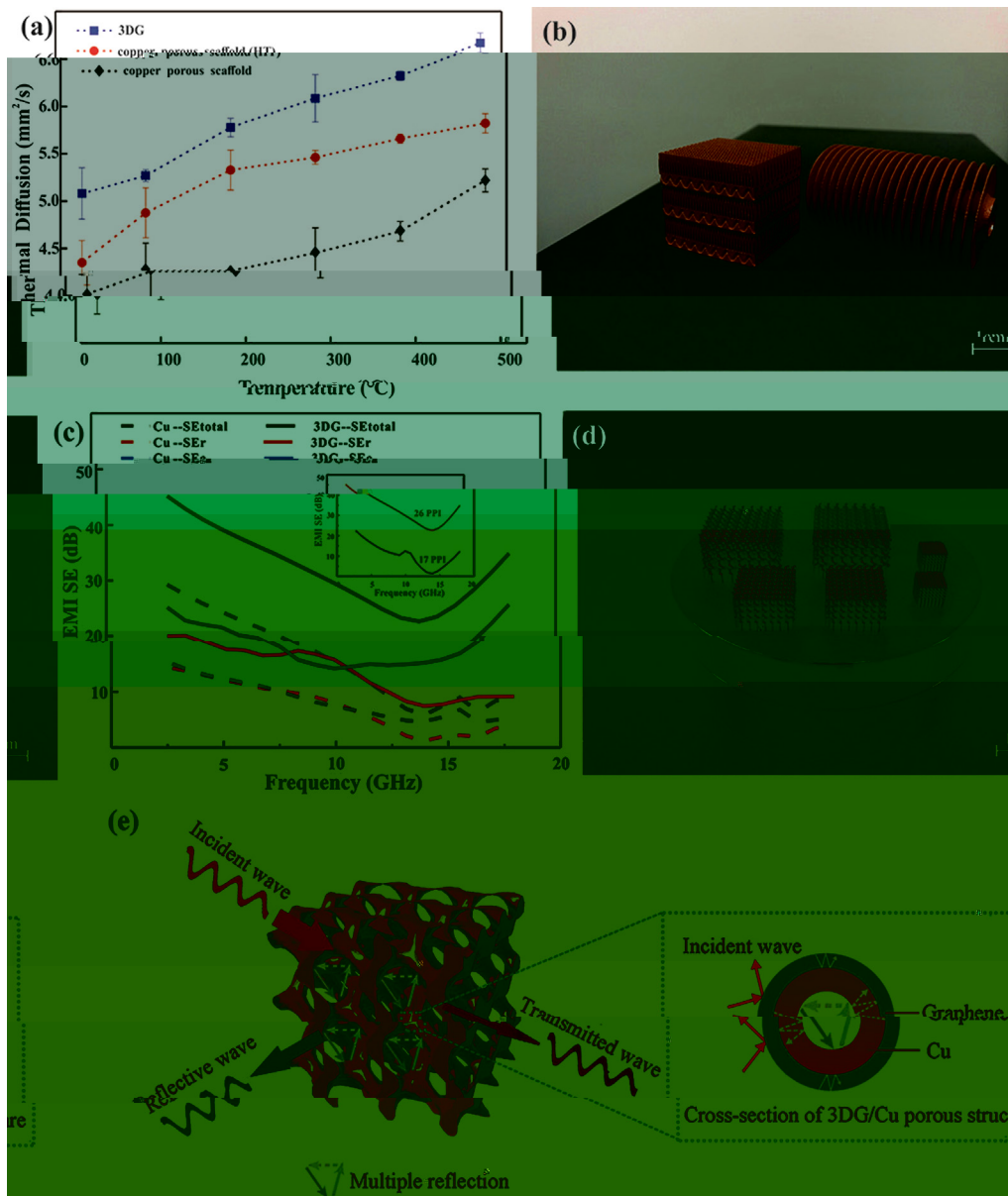


Fig. 9. Performance of 3DG/C porous scaffold: (a) thermal diffusion; (b) SLM prepared porous structure; (c) EMI SE; (d) Cross section of porous structure; (e) Schematic of 3DG/C porous structure EMI. (For interpretation of the references to colour in this figure legend, the reader is referred to the web version of this article.)

Table 1

Comparison of the EMI shielding performance of porous structures with different materials and methods. The maximum shielding efficiency (SE) and improvement of thermal property are listed in the table.

Coating materials	Substrate	Method	Maximum shielding efficiency (dB)	Improvement of thermal property (%)	Ref
G	Al	Infiltration + freeze-drying + sintering	37	-	50]
G	PS	Hydrothermal synthesis + sintering	29.3	-	56]
G	PMMA	Sol-gel + freeze-drying + sintering	19	-	57]
C /G	/C	Sol-gel + freeze-drying + sintering	-	8.5	58]
G	Ni	Freeze-drying + CVD	-	554	59]
G	C-Ni	Electrodeposition + freeze-drying + sintering	20	-	60]
G	C	Pre-sintering + CVD	-	2.4	61]
G	Al	Freeze-drying + sintering	47	6.3	62]
G	C	CVD + SLM	47.8	27	This work

Note: Poly (ethylene glycol)-PPMA, Polystyrene-PS.

Declaration of Competing Interest

The authors declare that they have no competing interests.

Acknowledgement

The authors thank the following for their financial support: National Natural Science Foundation of China (Nos. 51671091, No. 51902295, No. 51675496). The authors thank the following for their support: Faculty of Resources Environment and Urban Engineering, University of Geosciences (Wuhan) (Nos. (No. CUG170677) Humanities and Social Sciences Research Project (No. 2019 CFB264).

Appendix A. Supplementary data

Supplementary data for this article is available at <https://doi.org/10.1016/j.jes.2020.105904>.

References

1] B. J. R. G., N. N., M. T. P. S., Y. K., M. L., S. G. ... *Journal of Environmental Science and Technology* 2018;91:24-69.

2] B. J. R. G., A. G. S., B. W., C. H. L., T. J. D., M. F., T. J. S. ... *Journal of Environmental Science and Technology* 2008;8(3):902-7.

3] Li, H., C. S. M., P. J. H., P. O., S. T. J. G., T. J. I. S. ... *Journal of Environmental Science and Technology* 2016;8(36):24112-22.

4] K. M., K. J., J. B. C., K. J. H., A. J. H. G. ... *Journal of Environmental Science and Technology* 2017;11(8):7950-7.

5] P. J. C., M. H. M., T. M., L. D. P. ... *Journal of Environmental Science and Technology* 2020;262:118266-76.

6] Li, J., W. C., L. L., J. S. H., W. G., L. J. F. ... *Journal of Environmental Science and Technology* 2017;101:50-8.

7] H. Q., L. S. W., C. L. H., J. S. H., H. Q. S. ... *Journal of Environmental Science and Technology* 2018;6(42):21216-24.

8] D. S. T. M., S. T. P., D. S. T. P., K. T. J., K. M., A. S. T., T. J. 3D ... *Journal of Environmental Science and Technology* 2017;1(4):467-70.

9] Q. L., L. L., T. J. S. H., S. H., W. G., L. J. F. ... *Journal of Environmental Science and Technology* 2014;4(72):38273-80.

10] D. S. T. M., H. L. S. P., N. W. J. G. 3D ... *Journal of Environmental Science and Technology* 2016;90:424-32.

11] Li, L., W. S., C. Q., H. M. K., H. L. D., W. J. S. ... *Journal of Environmental Science and Technology* 2018. <https://doi.org/10.1002/f.201803938>.

12] Li, J., P. J., C. R. G., N. T. S. D., T. J. G. ... *Journal of Environmental Science and Technology* 2013;7(7):6001-6.

13] J. S. H., A. J. S. G., A. L. E. ... *Journal of Environmental Science and Technology* 2017;56:15520-38.

14] Ite, T., S. K., K. S. M., T. S. T., T. J. K., T. J. T. ... *Journal of Environmental Science and Technology* 2018;20(9):6024-33.

15] S. K., D. T. N., M. J. C., V. S. J. N., E. J. T. ... *Journal of Environmental Science and Technology* 2002;149(8):370-7.

16] C. H. S., M. S. W. L., G. H. Q., T. J. P. ... *Journal of Environmental Science and Technology* 2011;7(22):3163-8.

17] K. S. H., G. M., J. S. L., H. J. W., C. C. M. U. ... *Journal of Environmental Science and Technology* 2019;1(4):1077-87.

18] S. Q., F. L., L. W., L. H., L. J., T. J. C. ... *Journal of Environmental Science and Technology* 2017;29(31):1701583-90.

19] G. C., L. T. H., D. W., T. J. T. ... *Journal of Environmental Science and Technology* 2019. <https://doi.org/10.1021/s.9.08191>.

20] C. C. H., B. J., N. J. C., S. L. F., T. J. 3D ... *Journal of Environmental Science and Technology* 2019;175:107824-33.

21] St.čić J., B.žić D. T. ... *Journal of Environmental Science and Technology* 2016;307:407-17.

22] R. D. C., H. B., L. J., L. S. J., J. W., R. T. J. M. ... *Journal of Environmental Science and Technology* 2020;771:138586-95.

23] Li, C. W., A. J. K. S., N. J. D., T. J. L. ... *Journal of Environmental Science and Technology* 2009;324(5932):1312-4.

24] C. P., R. W. C., G. L. B., L. B. L., P. S. E., C. H. M. T. ... *Journal of Environmental Science and Technology* 2011;10:424-8.

25] J. S. D., D. S. S., G. S. S., L. K. T. J. P., H. J. V. ... *Journal of Environmental Science and Technology* 2019;270:47-58.

26] W. H. E. L., L. T. D., C. J. Q., F. T. J. E. ... *Journal of Environmental Science and Technology* 2019;170:107697-708.

27] G. D. D., M. S. W., W. S. K., P. R. L. S. ... *Journal of Environmental Science and Technology* 2013;57(3):133-64.

28] Li, E., T. S. C., S. L. L., F. T. A. E. ... *Journal of Environmental Science and Technology* 2017;249:255-63.

29] S. W. S., W. L. J., W. P. C., T. J. F. ... *Journal of Environmental Science and Technology* 2018;124:685-98.

30] Li, M. S., D. W. S., C. I. S. T. I. T. E. ... *Journal of Environmental Science and Technology* 2015;87:797-806.

31] L. C. L. A., M. S. S., T. M. A., T. R. C., W. S. P. J., L. P. D. T. ... *Journal of Environmental Science and Technology* 2019;166:294-305.

32] T. K., T. W. Q., T. J. D., S. S. M., M. J. D., T. J. R. ... *Journal of Environmental Science and Technology* 2016;6:26039-48.

33] K. H. T., P. L. N. H., T. S. B., C. K. G. ... *Journal of Environmental Science and Technology* 2016;11(3):183-91.

34] R. H. K., K. T. N. V., G. H. S., T. L. S., T. B. E. M. ... *Journal of Environmental Science and Technology* 2013;22(12):3872-83.

35] T. K., T. J. V., S. G. P. I. Q., G. T. J. A. ... *Journal of Environmental Science and Technology* 2015;646:303-9.

36] R. D. A., M. L. E., M. T. H., T. J. N. ... *Journal of Environmental Science and Technology* 2011;59(10):4088-99.

37] W. H. E. F. T. Y. S. T. H. ... *Journal of Environmental Science and Technology* 2018;743:258-61.

38] K. S. W. J. T. Y. S. E. T. I. E. 2003;23:309-48.

39] Li, G., G. S. J. F. Y. R., G. S. N. T. P. E. T. I. J. ... *Journal of Environmental Science and Technology* 2010;10(9):3512-6.

40] Li, S. C. I. W. W., C. L. L., R. E. F. R. Y. S. E. ... *Journal of Environmental Science and Technology* 2009;9(12):4268-72.

41] W. C., W. H., L. S. Q., L. A. S. J. J. ... *Journal of Environmental Science and Technology* 2020;161:479-85.

42] F. A. C., M. Y. J. C., S. V., C. S. I. C., L. M., M. F., T. J. R. ... *Journal of Environmental Science and Technology* 2006;97(18):187401-4.

43] S. G., J. S. H., F. P. C., H. Q. F. ... *Journal of Environmental Science and Technology* 2017;200:97-100.

44] J. K., E. H., J. C. J., D. I. F. I. T. E. ... *Journal of Environmental Science and Technology* 2014;311:351-6.

45] R. J. K., M. J. D. P., A. S. C., M. S., S. S. K. E. ... *Journal of Environmental Science and Technology* 2018;12:475-84.

46] S. B., L. W., W. C. S. J. ... *Journal of Environmental Science and Technology* 2016;8(12):8050-7.

47]

Mt 2019;34(5):489–98.

53] W B, C M, L M. R. <https://doi.org/10.1016/j.compositesa.2014.06.009>. A Mt 2014;26:3484–9.

54] C H, W S, J J, C J, et al. Synthesis of Fe₃O₄ nanoparticles by sol-gel method. *Compos Part A* 2019;121:139–48.

55] W L, J, Q. T. Effect of MWCNTs on the properties of epoxy resin. *J Mater Sci: Mater Electron* 2015;26(3):1895–9.

56] D G, P G, H P, Q F, M B, et al. ML Efficiently Predicts the Mechanical Properties of Nanocomposites. *J Mater Chem C* 2012;22:18772–4.

57] H B, Q, W G, H, et al. The effect of MWCNTs on the properties of epoxy resin. *ACS Appl Mater Interfaces* 2011;3:918–24.

58] S A, U N, T V. T. <https://doi.org/10.1051/comp/2016021>. *Mater Res Express* 2016. <https://doi.org/10.1051/comp/2016021>.

59] P M, J H, R S, S L. T. <https://doi.org/10.1016/j.compositesa.2012.12.009>. *Compos Part A* 2012;12:2959–64.

60] J K, H H, D P, et al. <https://doi.org/10.1016/j.compositesa.2017.12.009>. *Compos Part A* 2017;122:244–7.

61] R H, L S, B S, K T, W L, D S, L H, et al. <https://doi.org/10.1038/s41598-015-02710-1>. *Nature* 2015. <https://doi.org/10.1038/s41598-015-02710-1>.

62] T, F S, G L, G Q, L G, R K, et al. <https://doi.org/10.1016/j.compositesa.2019.105670>. *Compos Part A* 2019. <https://doi.org/10.1016/j.compositesa.2019.105670>.

63] R D, M L, M E, H D, M J, M B, et al. <https://doi.org/10.1016/j.compositesa.2011.09.009>. *Compos Part A* 2011;59(10):4088–99.

64] E S, S F, L K, S V, M C. T. <https://doi.org/10.1016/j.compositesa.1973.01.009>. *Compos Part A* 1973;1(1):10–38.